frontiers in Materials

ORIGINAL RESEARCH
published: 30 October 2020
doi: 10.3389/fmats.2020.520630

Martensitic Transition, Magnetic, Microstructural and Exchange Bias Properties of Melt Spun Ribbons of Mn-Ni-Sn Shape Memory Heusler Alloy

Jyoti Sharma[1], K. G. Suresh[2], M. Manivel Raja[3] and Pravin Walke[1]*

[1]National Centre for Nanosciences and Nanotechnology, University of Mumbai, Mumbai, India, [2]Department of Physics, Indian Institute of Technology Bombay, Mumbai, India, [3]Defence Metallurgical Research Laboratory, Hyderabad, India

In the present report, we have studied the structural, microstructural, magnetic, exchange bias (EB) properties and magnetoresistance (MR) in Mn rich (Mn at. ~50%) $Mn_{50}Ni_{50-x}Sn_x$ (x = 10) shape memory Heusler alloy ribbons, prepared using the melt spinning method. These ribbons were found to exhibit a first order structural (i.e., martensitic) transition at around 205 K from the high temperature austenite to the low temperature martensite phase. The martensitic transition occurs at comparatively lower temperatures in these ribbons than in the same bulk alloy. Curie temperature of the austenite phase (T_C^A) is found to be larger i.e., around room temperature than that of bulk alloy. A significant EB field (H_{EB}) of around 960 Oe has been observed at 2 K for these ribbons, which is found to be comparable to that reported for other Heusler systems. The presence of the EB effect in these ribbons is attributed to the coexistence of FM/AFM exchange interactions in the martensite phase. They are also found to show a maximum negative MR of around 12% near the martensitic transition, for 50 kOe field change. Investigation of DC magnetization, AC susceptibility measurements and the observation of training effect (i.e., characteristic feature of EB) strongly corroborates with the coexistence of FM/AFM exchange interactions in the martensite phase of these ribbons, which results in the large EB. The effects of temperature and magnetic field on the EB properties and MR have also been studied here.

Keywords: martensitic transition, exchange bias effect, magnetoresistance, ferromagnetic shape memory alloys, heusler alloys

OPEN ACCESS

Edited by:
Bhaskar R. Sathe,
Dr. Babasaheb Ambedkar Marathwada University, India

Reviewed by:
Dattatray Late,
National Chemical Laboratory (CSIR), India
Sanjay Singh,
Indian Institute of Technology (BHU), India

****Correspondence:***
Jyoti Sharma
jsharma628@gmail.com

Specialty section:
This article was submitted to Smart Materials, a section of the journal Frontiers in Materials

Received: *16 December 2019*
Accepted: *09 September 2020*
Published: *30 October 2020*

Citation:
Sharma J, Suresh KG, Raja MM and Walke P (2020) Martensitic Transition, Magnetic, Microstructural and Exchange Bias Properties of Melt Spun Ribbons of Mn-Ni-Sn Shape Memory Heusler Alloy. Front. Mater. 11:520630. doi: 10.3389/fmats.2020.520630

INTRODUCTION

In recent years, Ni rich (Ni at. ~50%) Ni-Mn-Z (Z = Ga, Sb, In, and Sn) shape memory full Heusler alloys have attracted a lot of attention within the research community, owing to their multifunctional properties such as large shape memory effect, exchange bias (EB), giant magnetoresistance and large magnetocaloric effect, etc. (Ullakko et al., 1996; Pasquale et al., 2005; Khan et al., 2007; Pathak et al., 2010). These properties have been exploited in various applications such as in shape memory devices, magnetic tunnel junctions, sensors, storage and spintronic devices, etc. (Meiklejohn and Bean, 1956; Parkin et al., 1999; Marioni et al., 2005; Wang et al., 2010; Graf et al., 2011). Most of these properties are found to be associated with their first order structural transition (i.e., the martensitic transition)

from the high temperature cubic austenite phase to the low temperature tetragonal/orthorhombic/monoclinic martensite phase. Meiklejohn and Bean in 1956 discovered the EB effect at the ferromagnetic (FM)/antiferromagnetic (AFM) interface between the Co particles as FM core embedded in the CoO as AFM shell (Meiklejohn and Bean, 1956). EB is seen to arise due to the unidirectional anisotropy created at the different kind of interfaces such as FM/AFM, AFM/ferrimagnetic, FM/spin glass (SG) or ferrimagnetic/SG, when the material is cooled in presence of magnetic field, to the low temperatures (Parkin et al., 1999; Khan et al., 2007; Sharma and Suresh, 2015b). EB can be described by the magnetic hysteresis (M–H) loop shifting along the magnetic field axis, when it is recorded after the field cooling (FC) process. It can be estimated from the quantity called the EB field (H_{EB})) (Meiklejohn and Bean, 1956), for example, a maximum H_{EB} of 248 Oe has been reported in Ni rich $Ni_{50}Mn_{25+x}Sb_{25-x}$, 377 Oe in $Ni_{50-x}Mn_{37+x}Sn_{13}$ Heusler alloy and 120 Oe in $Ni_{50}Mn_{50-x}In_x$ alloy at 5 K (Khan et al., 2007; Nayak et al., 2009; Pathak et al., 2009). In contrast to the Ni rich Heusler alloys, to date Mn rich (Mn at. ~50%) Mn-Ni-Z (Z = Ga, In and Sn) shape memory Heusler alloys have been extensively studied mostly in bulk form (Xuan et al., 2010; Bachaga et al., 2015; Sharma and Suresh, 2015a; Sharma et al., 2019). The melt spinning method is seen as an effective tool to prepare the polycrystalline samples of these alloys with higher homogeneity, very refined, reduced sized and highly textured microstructure, which may result in the enhancement of various physical properties as discussed above. In literature, there are many reports available on martensitic transition, magnetic, structural, microstructural, magnetocaloric and EB properties of Ni rich Ni-Mn-Z (Z = Ga, Sb, In, and Sn) Heusler alloys ribbons (Llamazares Sánchez et al., 2013; Wang et al., 2013; Zhao G. X. et al., 2013; Maziarz et al., 2014; Chen et al., 2015; Huu et al., 2015; Louidi et al., 2018). However, Mn rich Heusler alloys in their melt spun ribbon form have not been extensively studied so far.

It is reported in literature that the magnetic properties of these shape memory Heusler alloys strongly depend upon the Mn-Mn exchange interactions. In Mn rich full Heusler alloys, excess Mn atoms have been found to occupy not only the Z sites but also the Ni sites in the lattice, which generally couple antiferromagnetically with Mn atoms at the regular sites (Wijn, 1988; Xuan et al., 2010). At the same time, the first order martensitic transition further leads to the decrease in the distance between Mn atoms at regular sites and the Mn atoms at neighboring sites (i.e., at Ni and Z sites) due to the twinning of the martensite phase variants, which further leads to the enhancement of AFM coupling in the system. Excess of Mn content in the Mn-Ni-Z alloys is thought to be responsible for the differences in physical properties observed between Mn rich and Ni rich Heusler alloys, as mostly the Mn content contributed to the magnetism of these alloys. In the present report, we have investigated the martensitic transition, magnetic, structural, microstructural, EB properties and magnetoresistance in Mn rich $Mn_{50}Ni_{50-x}Sn_x$ (x = 10) Heusler alloy melt spun ribbons.

EXPERIMENTAL CHARACTERIZATION

A polycrystalline sample of the presented $Mn_{50}Ni_{50-x}Sn_x$ (x = 10) Heusler alloy was prepared by arc melting method in the presence of highly pure argon atmosphere, by taking the stoichiometric amount of high purity elements such as Mn, Ni, and Sn. The sample was melted several times to get the homogeneity. The weight loss after melting was found to be less than 1%. After melting, the sample was annealed at 1073 K for 72 h in a sealed quartz tube, and subsequently quenched in liquid nitrogen in order to achieve better homogeneity. After that the annealed sample was taken in a quartz tube (i.e., of 1 mm diameter nozzle), and melted in the induction furnace in presence of highly pure argon atmosphere. Following this, the molten alloy was ejected through the nozzle onto a rotating wheel (made up of Cu) and made to cool rapidly, which gave the melt spun ribbons. The ejection rate of the ribbons can be changed by changing the argon gas pressure accordingly. A typical arrangement for the melt spinning process is shown in the **Figure 1**. The structural analysis for these melt spun ribbons is performed by collecting the X-ray diffraction pattern at room temperature (RT) using a PANalytical X'pert PRO diffractometer. The qualitative and the quantitative microstructural analyses were performed by scanning electron microscopy (ESEM-FEI quanta 200 model) and energy dispersive spectroscopy (EDS arrangement attached with ESEM) respectively. The magnetization measurements have been performed by using a superconducting quantum interference device magnetometer (SQUID) (Quantum Design). Magnetization as a function of temperature was recorded in zero (ZFC), FC and field heating (FH) modes. In all these modes, the sample was cooled down to 2 K from 400 K. The resistivity measurements were carried out in a vibrating sample magnetometer attached with the physical property measurement system using a four probe method.

RESULTS AND DISCUSSION

Structural and Microstructural Analysis

Figure 2 shows the RT XRD pattern for $Mn_{50}Ni_{50-x}Sn_x$ (x = 10) Heusler alloy melt spun ribbons. From the refinement (using Fullproof software), it is found that these ribbons exhibit the cubic structure at RT, with the estimated lattice parameter (a = b = c) of around 5.99 Å. The lattice parameters for ribbons are found to be almost the same as that for the same bulk sample (a = b = c = ~6.00 Å), which suggests that average size of the crystallites will be nearly the same in both of the samples. The absence of (111) peak in the XRD pattern suggests that there may be disorder present in these ribbons (Graf et al., 2011). The observation of cubic structure at RT (i.e. the austenite phase structure) indicates that their martensitic transition lies below RT. Generally the structure of the Heusler alloys is made up of four interpenetrating fcc lattices, which have the Wyckoff positions namely 4a(0,0,0), 4b(1/2,1/2,1/2), 4c(1/4,1/4,1/4) and 4d(3/4,3/4, 3/4) (Graf et al., 2011). The preferred site occupancy of 3d elements in Ni-Mn based Heusler alloys is decided by their number of valence electrons, such as the 3d elements having more

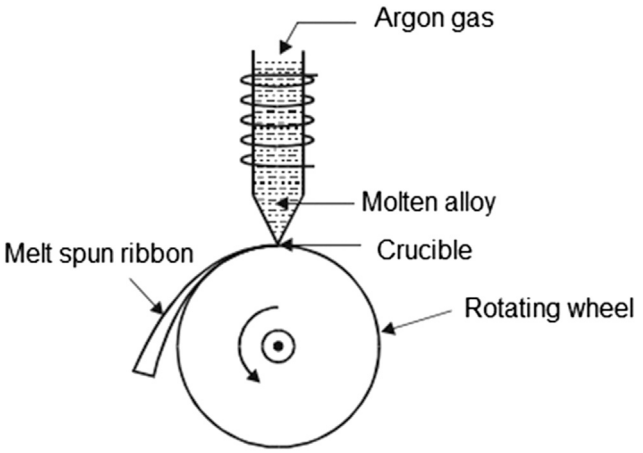

FIGURE 1 | A schematic diagram of the melt spinning method.

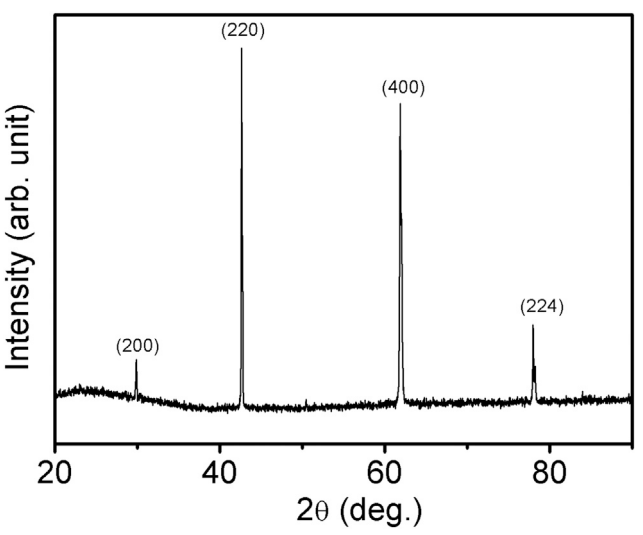

FIGURE 2 | Room temperature XRD pattern for the $Mn_{50}Ni_{50-x}Sn_x$ (x = 10) Heusler alloy melt spun ribbons.

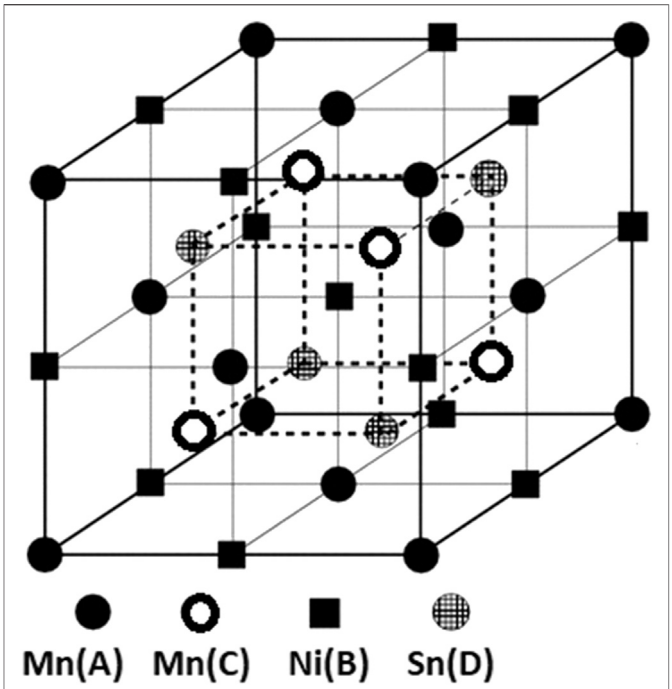

FIGURE 3 | A schematic cubic unit cell comprising of four interpenetrating fcc lattices, along with the expected site occupancies of different atoms.

valence electrons than Mn, prefer to occupy the 4a and 4b sites, and the structure is called Cu_2MnAl (regular) type. On the other hand, the 3d elements, which have the lesser valence electrons than Mn, prefer to occupy the 4a and 4c sites, and structure is known as Hg_2CuTi (inverse Heusler) type (Graf et al., 2011). Therefore, for a better understanding, a schematic of the cubic unit cell of present Heusler ribbons along with the Wyckoff positions of different atoms is shown in **Figure 3**. In the present case, Mn atoms are expected to occupy the 4a(0, 0, 0) and 4c(1/4,1/4,1/4) sites, which are denoted as the regular Mn atoms i.e., Mn(A) and Mn(C) respectively. Whereas Ni atoms occupy the 4b(1/2,1/2,1/2) sites, and Sn atoms occupy the 4d(3/4,3/4, 3/4) sites, which are denoted as Ni(B) and Sn(D) respectively. Generally it is seen in literature that, in Mn rich Heusler alloys, excess Mn atoms randomly occupy the Sn sites as well as the Ni sites, which suggests the presence of disorder in these systems, and consequently affects their electronic and magnetic properties (Xuan et al., 2010; Graf et al., 2011). The estimated nearest and next nearest inter-atomic distances (i.e., $\sqrt{3}a/4$ and $a/2$ Å respectively) between the Mn atoms suggest that there would be coexistence of AFM and FM coupling in the present ribbons.

Figure 4A,B shows the RT SEM images for the present melt spun ribbons, recorded at different areas of its free surface. It can be seen from the figure that these ribbons show a coarse granular microstructure, which consist of multiple shape grains (such as small columnar grains and tree leafs-like grains). No elongated thin plates and strips corresponding to the martensitic twin variants have been found inside the grains, this again confirm that the martensitic phase lies below the RT for these ribbons, which is in agreement with the XRD results. The average size of the grains lie between around 1–5 μm, which can be attributed to the different grain growth dynamics as a result of rapid solidification process. EDS analysis has also been performed on these ribbons (figure is not shown here), which confirmed the homogeneous composition throughout the sample. The chemical composition for these ribbons is found to be $Mn_{48.78}Ni_{40.76}Sn_{10.46}$. Standard deviation in elemental chemical composition obtained from EDS analysis is around 1.22 at. % for Mn, 0.76 at. % for Ni and 0.46 at. % for Sn respectively.

DC Magnetization Measurements

Figure 5 shows the magnetization as a function of temperature (M-T) curves for present ribbons in ZFC, FC and FH modes, measured in presence of 1 kOe field. It can be seen from the figure that the ribbon undergoes a first order structural (i.e., called

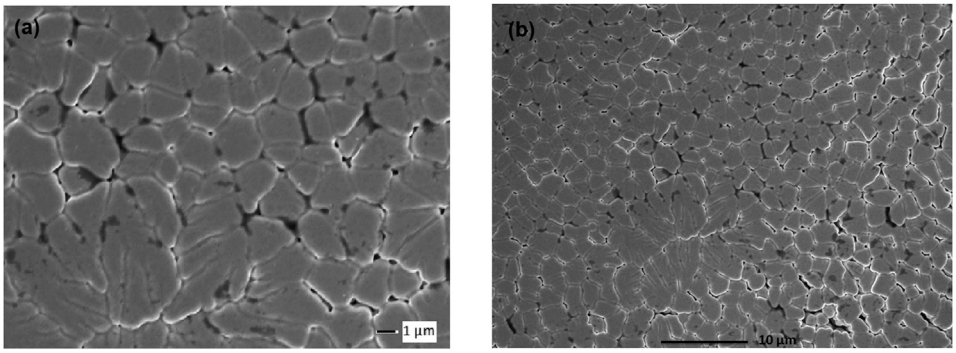

FIGURE 4 | (A,B) Room temperature SEM micrographs of these melt spun ribbons collected at different areas of its free surface.

martensitic) transition at around 205 K with a sudden increase in magnetization value (i.e., the maximum magnetization value), which corresponds to martensitic start temperature (M_s). It gets the minimum magnetization value at around 165 K, which corresponds to martensitic finish temperature (M_f). This corresponds to the forward martensitic transition. Similarly, we can notify the martensitic transition in terms of austenite start temperature (A_s) and the austenite finish temperature (A_f), as also marked in the **Figure 5**, that corresponds to the reverse martensitic transition. Curie temperature of austenite phase (T_C^A) occurs at around RT. As the temperature decreases below M_f, the magnetization starts to increase again, and ZFC, FC M-T curves show splitting at around 120 K. The ZFC curve shows a hump at around 66 K followed by that ZFC magnetization decreases with the further decrease in temperature down to 2 K. This splitting suggests the presence of the magnetic frustration at low temperatures in the martensite phase, which may be due to the presence of SG or coexistence of AFM/FM exchange interactions in these ribbons (Giri et al., 2011; Sharma and Suresh, 2015b). The first order nature of the martensitic transition is confirmed by the hysteresis observed between FC and FH M-T curves. The martensitic transition temperatures for these ribbons are found to be lower than that for the same bulk alloy, as M_s and M_f for the bulk composition are around 228 and 171 K respectively. Whereas T_C^A for the ribbons (i.e., around RT) is found to be higher than that for the bulk alloy (i.e., T_C^A = 278 K) (Sharma and Suresh, 2015a). The decrease in the martensitic transition temperatures for these ribbons comparative to the bulk composition may be attributed to the change in exchange interactions, as a result of the change in grain size after rapid solidification process. **Table 1** shows the better comparison of different martensitic transition temperatures observed in other Heusler alloys ribbons with the present case. One can see from the **Table 1** that the observed values of martensitic transition temperatures in the present case are in agreement with those obtained for other Heusler ribbons (Rama Rao et al., 2007; Maziarz et al., 2013; González-Legarreta et al., 2015).

To study the nature of the low temperature frustrated magnetic state of these ribbons, AC susceptibility as a function of temperature has been measured, at different frequencies

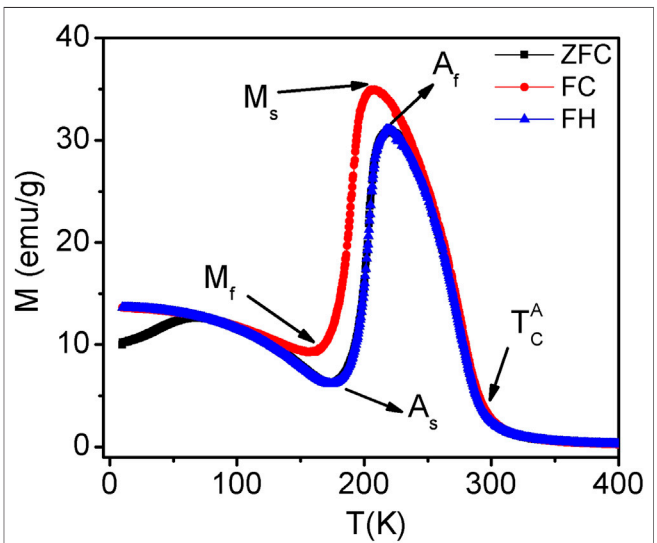

FIGURE 5 | The ZFC, FC and FH, magnetization as a function of temperature (M-T) curves measured at 1 kOe field.

ranging from 10 to 995 Hz, such as the data is shown in the **Figure 6**. It can be seen from the figure that at 10 Hz frequency, there is broad peak observed at around 150 K (marked as T_P in the figure), which occurs at a significantly higher temperature than that observed in DC M-T curve (**Figure 5**). A small frequency dependence of this peak at 250 Hz can be seen from the figure, but it is not measurable due to the broadness of the peak. Whereas for higher frequencies, there is no prominent frequency dependence observed for this peak, which rules out the possibility of a SG phase in these ribbons. Therefore the low temperature martensite phase is expected to consist of the mixed FM/AFM phases, which was expected and discussed earlier.

Exchange Bias Properties

As we have discussed from the DC magnetization and AC susceptibility measurements, there is a coexistence of FM/AFM phases in the martensite phase, which can lead to the EB effect. Therefore, to investigate the EB effect in the present ribbons, we

TABLE 1 | Comparison of various martensitic transition temperatures obtained for other Heusler alloys ribbons reported in literature with the present ribbons.

Alloy (composition)	M_s (K)	M_f (K)	$T_{A-M} = (M_s + M_f)/2$(K)	A_s (K)	A_f (K)	$T_{M-A} = (A_s + A_f)/2$ (K)	T_C^A (K)	Ref.
$Ni_{47}Mn_{41}In_{12}$	185	110	148	194	223	209	292	González-Legarreta et al. (2015)
$Ni_{53}Mn_{20.4}Ga_{26.6}$	185	178	182	190	198	194	306	Rama Rao et al. (2007)
$Ni_{48}Mn_{39.5}Sn_{12.5}$	—	—	242	—	—	258	300	Maziarz et al. (2013)
Present alloy	205	165	185	174	218	196	284	—

have collected the magnetic hysteresis (M-H) loop at 2 K in field range of ±20 kOe, after FC the sample in presence of 10 kOe. The M-H hysteresis loop at 2 K is shown in **Figure 7** in the field range of ±8 kOe for better visibility of M-H loop shifting. It is clear from the figure that the M-H loop completely shifts towards the negative field axis, which confirms the EB effect in these ribbons. A maximum value of exchange bias field (H_{EB}) of around 960 Oe has been estimated at 2 K, which is found to be comparable to that reported in other Heusler systems (Pathak et al., 2009; Xuan et al., 2010; Sahoo et al., 2013; Zhao G. X. et al., 2013; Zhao X. G. et al., 2013; Czaja et al., 2014; Sharma and Suresh, 2015a). The present ribbons are found to show improved EB as compared to the same bulk composition (as H_{EB} = 920 Oe) at the same temperature and cooling field conditions, which may be attributed the change in the strength of AFM/FM exchange interactions as a result of the change in Mn-Mn inter-atomic distances (Sharma and Suresh, 2015a). Similarly, the present ribbons also show the relatively larger EB than that observed in other related Heusler alloys ribbons, such as in $Ni_{50}Mn_{37}Sn_{13}$ ribbons (H_{EB} = ~225 Oe at 5 K), in $Ni_{45.5}Mn_{43.0}In_{11.5}$ ribbons (H_{EB} = 270 Oe at 5 K), in $Ni_{50}Mn_{38}Sn_{12}$ ribbons (H_{EB} = ~300 Oe at 5 K), in $Mn_{46}Ni_{42}Sn_{11}Sb_1$ ribbons (H_{EB} = 90 Oe at 50 K), and in $Mn_{50}Ni_{50-x}Sn_x$ (x = 11) Heusler ribbons (H_{EB} = ~213 Oe at 2 K) (Yang et al., 2012; Llamazares Sánchez et al., 2013; González-Legarreta et al., 2014; Huang et al., 2016; Sharma et al., 2020). The H_{EB} is calculated by using the formula $H_{EB} = -(H_1 + H_2)/2$, where the H_1 and H_2 are designated as the left and right coercive fields, where the magnetization vanishes. The presence of EB effect in these ribbons confirms the coexistence of FM/AFM phases at low temperatures in the martensite phase.

The training effect, which is a characteristic feature of EB, has also been investigated in the present ribbons. The training effect is defined by the decrease of EB field, when the field cooled M-H loop is repeated consecutively "n" (*n* = no. of cycles) times. To study the training effect, we have recorded M-H loops at 2 K in the consecutive field cycles (*n*), after FC the sample at 10 kOe (data not shown here). The estimated EB field, H_{EB} from these consecutive M-H loops at 2 K is shown in the inset of **Figure 7**, as a function of no. of cycles. It can be seen from the inset that H_{EB} is decreasing with the increase of *n*. This experimental data has been fitted to the simple power law (i.e., given by equation $H_{EB} - H_{EB\infty} \alpha 1/\sqrt{n}$, where $H_{EB\infty}$ is EB field in the asymptotic limit of *n*. It is clear from the inset that, our experimental data fits well with the simple power law (as shown by the solid line in the inset), and the estimated value of $H_{EB\infty}$ from the fit is around 946 Oe.

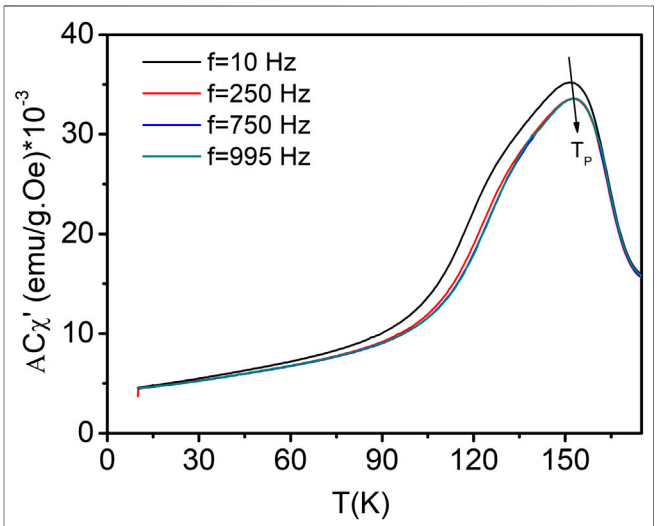

FIGURE 6 | Temperature dependence of the real part of AC susceptibility (χ′) measured at different frequencies for the present ribbons.

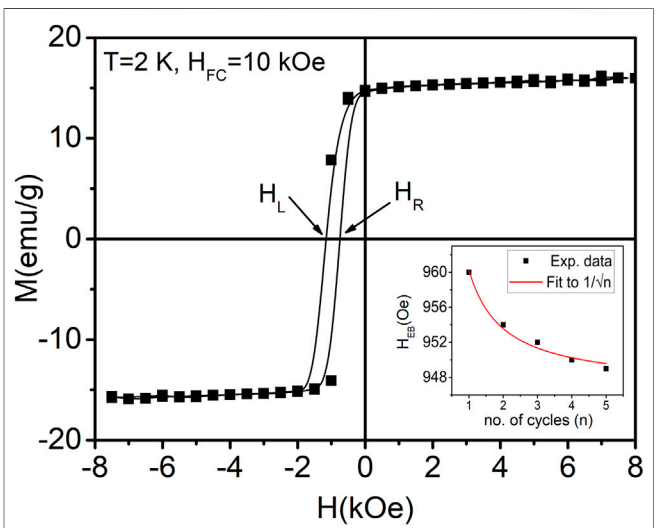

FIGURE 7 | EB effect: Magnetic hysteresis (M-H) loop measured at 2 K after field cooling process in presence of 10 kOe magnetic field. Inset shows the training effect of exchange bias observed in the present ribbons. Here solid squares show the experimental data and solid line shows the fit to simple power law ($H_{EB} - H_{EB\infty} \alpha 1/\sqrt{n}$).

Training effect is described by the fact that at the time of magnetization reversal in consecutive M-H loops, FM moments do not get reversed homogenously, which is attributed to the AFM moments rearrangement at the interfaces and this consequently results in the decrease of H_{EB} with increasing *n*.

To study the effect of temperature on EB properties, the magnetic hysteresis (M-H) loops have been recorded at different temperatures in a field range of ±20 kOe after the FC process in the presence of 10 kOe (data not shown here). The shifting of the M-H loop has been found to decrease with the increase of temperature, and vanishes at around 70 K, which corresponds to the EB blocking temperature (T_B), at which the AFM moments would not be able to pin the FM moments and consequently results in the zero EB field. The estimated value of the EB field from these M-H hysteresis loops as a function of temperature is shown in the **Figure 8**. The H_{EB} is found to decrease with increasing temperature, which may be attributed to the decrease in exchange coupling between the AFM/FM phases as a result of the increase in thermal energy. It can be noted that the present Heusler alloy ribbons show a large EB at the low temperatures, and retains the reasonable value upto around 40 K.

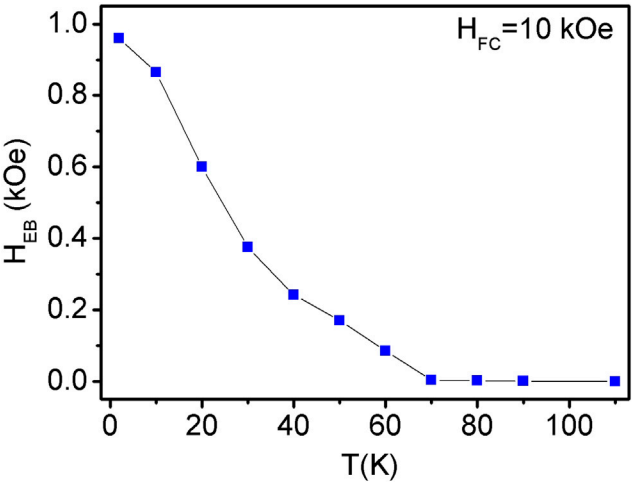

FIGURE 8 | Temperature dependence of the EB field (H_{EB}) estimated from the M-H loops recorded at different temperatures after field cooling at 10 kOe field.

Magnetoresistance

To shed more light onto the results obtained from the magnetization measurements near the first order martensitic transition of these ribbons, the electrical resistivity measurements have also been performed. The temperature dependence of resistivity (in heating and cooling modes) measured in presence of zero and 50 kOe field is shown in **Figure 9**. At higher temperatures i.e., in the austenite phase, ρ-T curves show a typical metallic behavior. As the temperature is lowered from 400 K, resistivity suddenly starts increasing and first order martensitic transition takes place. After reaching its maximum value, resistivity becomes almost constant with further lowering the temperature. The value of martensitic transition temperatures obtained from these ρ-T curves are in agreement with those obtained from the DC magnetization measurements (**Figure 5**). The hysteresis observed between the heating and cooling ρ-T curves again confirms the first order nature of the martensitic transition. It can be seen from the figure that with the application of magnetic field (50 kOe), the martensitic transition temperatures are found to decrease, which can be attributed to the fact that martensitic phase transformation gets hindered by the application of the magnetic field. At 50 kOe field, the austenite phase may not completely transform into the martensite phase i.e., the remaining phase gets kinetically arrested in the austenite state, which consequently leads to the shift in martensitic transition to lower temperature. The similar type of phenomenon i.e., kinetic arrest of the first-order martensitic transition from FM austenite phase to weakly magnetic/AFM phase has also been observed in many Heusler systems (Sharma et al., 2007; Xu et al., 2010). This implies that the application of magnetic field leads to the stabilization of the austenite phase in the present ribbons. To confirm the kinetic arrest behavior of the martensitic transition, the electrical resistivity as a function of magnetic field for the present ribbons has also been measured at

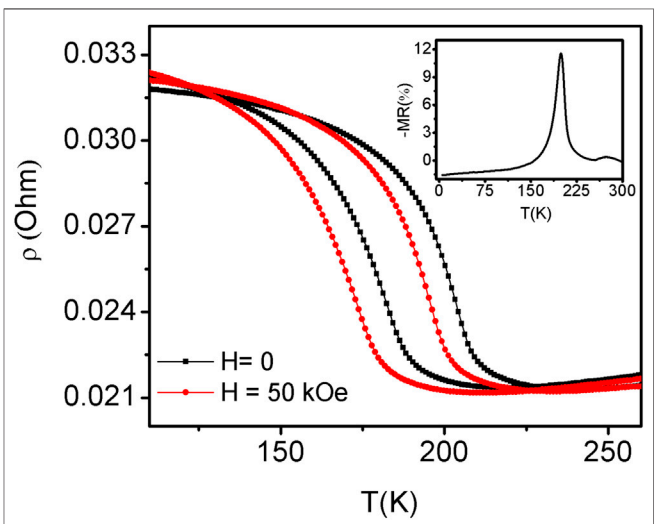

FIGURE 9 | Temperature as a function of resistivity (ρ), measured in zero and 50 kOe field. Inset shows the magnetoresistance (MR) as a function of temperature, calculated from these ρ-T curves.

various temperatures in the vicinity of martensitic transition (data not shown here). The results obtained from the $\rho(H)$ curves are found to be in agreement with those observed from $\rho(T)$ curves.

The magnetoresistance (i.e., the measure of change in resistivity with respect to the change in magnetic field) has also been calculated for the present ribbons using the resistivity data (**Figure 9**). MR (calculated by using the formula $(\rho(H) - \rho(0))/\rho(0) \times 100$) as a function of temperature for 50 kOe field change is shown in the inset of **Figure 9**. These ribbons are found to show a maximum negative MR of around 12% at 198 K for 50 kOe field change, which is comparable to that

obtained for other Heusler systems (Pathak et al., 2010; Sahoo et al., 2013). The observed MR in present ribbons is found to be larger as compared to that observed in the same bulk composition i.e., MR = −6.4% for same field change (Sharma et al., 2019). Similarly, a relative improvement in MR is also obtained in the present ribbons as compared to that observed in some other Heusler alloys ribbons, such as MR = −10% is obtained in Ni-Co-Mn-Sb as spun ribbons, and a maximum negative MR of 9% is obtained in Ni–Fe–Ga Heusler ribbons (Sahoo et al., 2013; Tolea et al., 2017). MR shows the maximum value near the martensitic transition temperature, as it arises due to the field induced nature of the first order martensitic transition.

SUMMARY

Here the first order martensitic transition, magnetic, structural, microstructural, EB properties and MR of $Mn_{50}Ni_{50-x}Sn_x$ (x = 10) shape memory Heusler alloy melt spun ribbons have been studied. These ribbons were prepared by melt spinning method. The RT structure is found to be cubic for these ribbons with the estimated lattice parameters (a = b = c) of 5.99 Å. They have been found to undergo a first order martensitic transition at around 205 K from the cubic austenite phase to the martensite phase, which is comparatively lower than that for the same bulk composition. This can be attributed to the change in strength of AFM/FM exchange interactions, as a result of the change in grain size during the melt spinning process. Curie temperature of the austenite phase (T_C^A) lies around RT. These ribbons show a significant EB effect with EB field of 960 Oe at 2 K, after FC in presence of 10 kOe, which is found to be relatively larger than that reported in some other Heusler systems. The H_{EB} decreases with the increase in temperature. The presence of EB in these melt spun ribbons can be attributed to the coexistence of FM/AFM exchange interactions in the martensite phase. DC magnetization, AC susceptibility measurements and the observation of training effect confirm the presence of coexistence of FM/AFM exchange interactions at low temperatures. They have also been found to show a maximum negative MR of 12% around the martensitic transition for 50 kOe field change. Resistivity measurements show that the application of a magnetic field leads to the stabilization of the austenite phase. Thus the present results suggest that the melt spinning may be used as an effective method of material preparation, so that various physical properties of Heusler alloys, such as the magnetic, magnetocaloric effect, EB and MR, etc. can be modified according to the fundamental research as well as from the application point of view.

DATA AVAILABILITY STATEMENT

The raw data supporting the conclusions of this article will be made available by the authors, without undue reservation, to any qualified researcher.

AUTHOR CONTRIBUTIONS

JS performed all the experiments shown in the manuscript. Melt spun ribbons were prepared at DMRL, hyderabad with the help of MR. JS discussed the results with KS and PW.

ACKNOWLEDGMENTS

Authors would like to acknowledge the SERB Govt. of India for the financial assistance granted through a national post doctoral fellowship (NPDF) project.

REFERENCES

Bachaga, T., Daly, R., Khitouni, M., Escoda, L., Saurinal, J., and Suño, J. J. (2015). Thermal and structural analysis of $Mn_{49.3}Ni_{43.7}Sn_{7.0}$ Heusler alloy ribbons. *Entropy* 17, 646–657. doi:10.3390/e17020646

Chen, X., Naik, B. V., Mahendiran, R., and Ramanujan, V. R. (2015). Optimization of Ni–Co–Mn–Sn Heusler alloy composition for near room temperature magnetic cooling. *J. Alloys Compd.* 618, 187–191. doi:10.1016/j.jallcom.2014.08.032

Czaja, P., Maziarz, W., Przewoznik, J., Kapusta, C., Hawelek, L., Chrobak, A., et al. (2014). Magnetocaloric properties and exchange bias effect in Al for Sn substituted $Ni_{48}Mn_{39.5}Sn_{12.5}$ Heusler alloy ribbons. *J. Magn. Magn. Mater.* 358–359, 142–148. doi:10.1016/j.jmmm.2014.01.069

Giri, C. S., Patra, M., and Majumdar, S. (2011). Exchange bias effect in alloys and compounds. *J. Phys. Condens. Matter.* 23, 073201. doi:10.1088/0953-8984/23/7/073201

González-Legarreta, L., González-Alonso, D., Rosa, W. O., Caballero-Flores, R., Suñol, J. J., González, J., et al. (2015). Magnetostructural phase transition in off-stoichiometric Ni–Mn–In Heusler alloy ribbons with low in content. *J. Magn. Magn. Mater.* 383, 190–195. doi:10.1016/j.jmmm.2014.10.152

González-Legarreta, L., Rosa, O.W., García, J., Ipatov, M., and Hernando, B. (2014). Annealing effect on the crystal structure and exchange bias in Heusler Ni45.5Mn43.0In11.5 alloy ribbons. *J. Alloys Compd.* 582, 588–593. doi:10.1016/j.jallcom.2013.08.078

Graf, T., Felser, C., and Parkin, S. S. P. (2011). Simple rules for the understanding of Heusler compounds. *Prog. Solid State Ch.* 39, 1–50. doi:10.1016/j.progsolidstchem.2011.02.001

Huang, Q., Chen, F., Zhang, M., and Xu, X. (2016). Magnetoresistance and exchange bias in high Mn content melt-spun $Mn_{46}Ni_{42}Sn_{11}Sb_1$ alloy ribbon. *Chin. Phys. B.* 25, 057305. doi:10.1088/1674-1056/25/5/057305

Huu, D. T., Yen, N. H., Thanh, P. T., Mai, N. T., Thanh, T. D., Phan, T. L, et al. (2015). Magnetic, magnetocaloric and critical properties of $Ni_{50-x}Cu_xMn_{37}Sn_{13}$ rapidly quenched ribbons. *J. Alloys Compd.* 622, 535–540. doi:10.1016/j.jallcom.2014.10.126

Khan, M., Dubenko, I., Stadler, S., and Ali, N. (2007). Exchange bias in bulk Mn rich Ni–Mn–Sn Heusler alloys. *Appl. Phys. Lett.* 91, 072510. doi:10.1063/1.2818016

Llamazares Sánchez, L. J., Flores-Zúñiga, H., Ríos-Jara, D., Sánchez-Valdes, F. C., García-Fernández, T., Ross, A. C., et al. (2013). Structural and magnetic characterization of the intermartensitic phase transition in NiMnSn Heusler alloy ribbons. *J. Appl. Phys.* 113, 17A948. doi:10.1063/1.4800836

Louidi, S., Sunol, J. J., Ipatov, M., and Hernando, B. (2018). Effect of cobalt doping on martensitic transformations and the magnetic properties of $Ni_{50-x}Co_xMn_{37}Sn_{13}$ (x = 1, 2, 3) Heusler ribbons. *J. Alloys Compd.* 739, 305–310. doi:10.1016/j.jallcom.2017.12.280

Marioni, M. A., O'Handley, R. C., Allen, S. M., Hall, S. R., Paul, D. I., Richard, M. L., et al. (2005). The ferromagnetic shape-memory effect in Ni–Mn–Ga. *J. Magn. Magn. Mater.* 290, 35. doi:10.1016/j.jmmm.2004.11.156

Maziarz, W., Czaja, P., Szczerba, M. J., Przewoźnik, J., Kapusta, C., Żywczak, A., et al. (2013). Room temperature magneto-structural transition in Al for Sn substituted Ni–Mn–Sn melt spun ribbons. *J. Magn. Magn. Mater.* 348, 8–16. doi:10.1016/j.jmmm.2013.08.005

Maziarz, W., Czaja, P., Szczerba, M. J., Przewoźnik, J., Kapusta, C., Żywczak, A., et al. (2014). Surface topography, microstructure and magnetic domains in Al for Sn substituted metamagnetic Ni-Mn-Sn Heusler alloy ribbons. *Intermetallics* 55, 1–8. doi:10.1016/j.intermet.2014.07.001

Meiklejohn, W. H., and Bean, C. P. (1956). New magnetic anisotropy. *Phys. Rev.* 102, 1413. doi:10.1103/PhysRev.102.1413

Nayak, A. K., Suresh, K. G., and Nigam, A. K. (2009), Observation of enhanced exchange bias behaviour in NiCoMnSb Heusler alloys. *J. Phys. D: Appl. Phys.* 42, 115004. doi:10.1088/0022-3727/42/11/115004

Parkin, S. S. P., Roche, K. P., Samant, M. G., Rice, P. M., Beyers, R. B., Scheuerlein, R. E., et al. (1999). Exchange-biased magnetic tunnel junctions and application to nonvolatile magnetic random access memory (invited). *J. Appl. Phys.* 85, 5828. doi:10.1063/1.369932

Pasquale, M., Sasso, C. P., Lewis, L. H., Giudici, L., Lograsso, T., and Schlagel, D. (2005). Magnetostructural transition and magnetocaloric effect in $Ni_{55}Mn_{20}Ga_{25}$ single crystals. *Phys. Rev. B* 72, 094435. doi:10.1103/PhysRevB.72.094435

Pathak, A. K., Dubenko, I., Pueblo, C., Stadler, S., and Ali, N. (2010). Magnetoresistance and magnetocaloric effect at a structural phase transition from a paramagnetic martensitic state to a paramagnetic austenitic state in $Ni_{50}Mn_{36.5}In_{13.5}$ Heusler alloys. *Appl. Phys. Lett.* 96, 172503. doi:10.1063/1.3422483

Pathak, A. K., Khan, M., Gautam, B. R., Stadler, S., Dubenko, I., and Ali, N. (2009). Exchange bias in bulk Ni–Mn–In-based Heusler alloys. *J. Magn. Magn. Mater.* 321, 963–965. doi:10.1016/j.jmmm.2008.03.008

Rama Rao, N. V., Gopalan, R., Manivel Raja, M., Chelvane, J. A., Majumdar, B., and Chandrasekaran, V. (2007). Magneto-structural transformation studies in melt-spun Ni–Mn–Ga ribbons. *Scr. Mater.* 56, 405–408. doi:10.1016/j.scriptamat.2006.10.037

Sahoo, R., Raj Kumar, M. D., Babu, A. D., Suresh, G. K., Nigam, K. A., and Raja, M. M. (2013). Effect of annealing on the magnetic, magnetocaloric and magnetoresistance properties of Ni-Co-Mn-Sb melt spun ribbons. *J. Magn. Magn. Mater.* 347, 95–100. doi:10.1016/j.jmmm.2013.07.027

Sharma, J., Coelho, A. A., Repaka, D. V. M., Ramanujan, R. V., and Suresh, K. G. (2019). Pressure induced martensitic transition, magnetocaloric and magneto-transport properties in Mn-Ni-Sn Heusler alloy. *J. Magn. Magn. Mater.* 487, 165307. doi:10.1016/j.jmmm.2019.165307

Sharma, J., Nag, J., Suresh, G. K., Manivel Raja, M., and Walke, P. (2020). Martensitic transition, magnetic and exchange bias properties in Mn rich Heusler alloy ribbons. *AIP Conf. Proc.* 2220, 110021. doi:10.1063/5.0001389

Sharma, J., and Suresh, K. G. (2015a). Investigation of multifunctional properties of $Mn_{50}Ni_{40-x}Co_xSn_{10}$ (x=0–6) Heusler alloys. *J. Alloys Compd.* 620, 329–336. doi:10.1016/j.jallcom.2014.09.141

Sharma, J., and Suresh, K. G. (2015b). Observation of giant exchange bias in bulk $Mn_{50}Ni_{42}Sn_8$ Heusler alloy. *Appl. Phys. Lett.* 106, 072405. doi:10.1063/1.4913268

Sharma, V. K., Chattopadhyay, M. K., and Roy, S. B. (2007). Kinetic arrest of the first order austenite to martensite phase transition in $Ni_{50}Mn_{34}In_{16}$: dc magnetization studies. *Phys. Rev. B.* 76, 140401. doi:10.1103/PhysRevB.76.140401

Tolea, F., Tolea, M., Sofronie, M., Popescu, B., Crisan, A., Leca, A., et al. (2017). Specific changes in the magnetoresistance of Ni–Fe–Ga Heusler alloys induced by Cu, Co, and Al substitutions. *IEEE Trans. Magn.* 53 (4), 1–7. doi:10.1109/TMAG.2016.2628386

Ullakko, K., Huang, J. K., Kantner, C., O'Handley, R. C., and Kokorin, V. V. (1996). Large magnetic-field-induced strains in Ni_2MnGa single crystals. *Appl. Phys. Lett.* 69, 1966. doi:10.1063/1.117637

Wang, W., Liu, E., Kodzuka, M., Sukegawa, H., Wojcik, M., Jedryka, E., et al. (2010). Coherent tunneling and giant tunneling magnetoresistance in Co2FeAl/MgO/CoFe magnetic tunneling junctions. *Phys. Rev. B.* 81, 140402. doi:10.1103/PhysRevB.81.140402

Wang, W., Yu, J., Zhai, Q., Luo, Z., and Zheng, H. (2013). Origin of retarded martensitic transformation in Heusler Ni-Mn-Sn melt-spun ribbons. *Intermetallics* 42, 126–129. doi:10.1016/j.intermet.2013.06.002

Wijn, H. R. J. (1988). *Alloys and compounds of d-elements with main group elements*. Editors P. J. Webster and K. R. A. Ziebeck (Berlin, Germany: Springer), Vol. 19/c.

Xu, X., Ito, W., Tokunaga, M., Umetsu, R. Y., Kainuma, R., and Ishida, K. (2010). Kinetic arrest of martensitic transformation in NiCoMnAl metamagnetic shape memory alloy. *Mater. Trans.* 51, 1357–1360. doi:10.2320/matertrans.M201009

Xuan, H. C., Cao, Q. Q., Zhang, C. L., Ma, S. C., Chen, S. Y., Wang, D. H., et al. (2010). Large exchange bias field in the Ni–Mn–Sn Heusler alloys with high content of Mn. *Appl. Phys. Lett.* 96, 202502. doi:10.1063/1.3428782

Yang, B. Y., Ma, B. X., Chen, G. X., Wei, Z. J., Wu, R., Han, Z. J., et al. (2012). Structure and exchange bias of $Ni_{50}Mn_{37}Sn_{13}$ ribbons. *J. Appl. Phys.* 111, 07A916. doi:10.1063/1.3672244

Zhao, G. X., Tong, M., Shih, W. C., Li, B., Chang, C. W., Liu, W., et al. (2013). Microstructure, martensitic transitions, magnetocaloric, and exchange bias properties in Fe-doped Ni-Mn-Sn melt-spun ribbons. *J. Appl. Phys.* 113, 17A913. doi:10.1063/1.4794881

Zhao, X. G., Hsieh, C. C., Lai, J. H., Cheng, X. J., Chang, W. C., Cui, W. B., et al. (2013). Effects of annealing on the magnetic entropy change and exchange bias behavior in melt-spun Ni-Mn-In ribbons. *Scr. Mater.* 63, 250–253. doi:10.1016/j.scriptamat.2010.03.067